CLM-P80

United Kingdom Atomic Energy Authority

RESEARCH GROUP

Preprint

HIGH VACUUM MEASUREMENT BY MEANS OF VIRTUAL CATHODE RELAXATION TIME

O. LLOYD

Culham Laboratory,

Culham, Abingdon, Berkshire

1965

HIGH VACUUM MEASUREMENT BY MEANS OF VIRTUAL CATHODE RELAXATION TIME

by

O. LLOYD*

(Submitted for publication in British Journal of Applied Physics)

A B S T R A C T

The theory of virtual cathode formation in electron beams is reviewed. Destruction of a virtual cathode by the accumulation of residual gas ions is shown to occur in a time which is inversely proportional to pressure. This forms the basis of a method of measuring low pressure which may have some advantages over conventional ionization gauges, especially in the presence of high magnetic fields.

Experimental results are presented where this effect is used to measure pressures in the range 10^{-4} to 4×10^{-9} Torr.

*Now at: C.E.G.B. Marchwood Laboratory, Nr. Southampton.

U.K.A.E.A. Research Group,
Culham Laboratory,
Nr. Abingdon,
Berks.

July, 1965. (C/7 MEA)

C O N T E N T S

1. INTRODUCTION

Neutralization of space charge in electron beams by ionization of residual gas is a well known effect. A special case occurs when the current density in a beam is sufficiently high to form a virtual cathode, which forms a three-dimensional potential well in which ions are trapped (Volosok and Chirikov 1957, Atkinson 1962; 1963). When sufficient ions have accumulated, their neutralizing effect brings about the sudden destruction of the virtual cathode, which can be detected as a pulse on an electrostatic probe. Under certain conditions the relaxation time is inversely proportional to pressure: this forms the basis for a practical method of measuring pressure in the high vacuum range.

2. VIRTUAL CATHODE FORMATION IN A ONE-DIMENSIONAL ELECTRON BEAM

Symmetrical Potential Distribution

Consider an electron beam of infinite extent in the x and y directions, moving in the z direction between two equipotential grids at $z = 0$ and $z = 2L$ (Fig.1a). When the current density j is low, the beam is completely transmitted and the potential distribution $V(z)$ can be found by integration of the one-dimensional Poisson equation (M.K.S. units):-

$$\frac{d^2V}{dz^2} = - \frac{j}{\varepsilon_o}\left(\frac{m}{2e}\right)^{\frac{1}{2}} V^{-\frac{1}{2}} , \qquad \ldots (1)$$

with boundary conditions $V = V_a$ (grid potential) at $z = 0$ and $z = 2L$.

The solution, which can be found in the literature (Bursian and Pavlov 1923), is symmetrical about $z = L$:-

$$\frac{j}{\varepsilon_o}\left(\frac{m}{2e}\right)^{\frac{1}{2}} z(z-2L) = 4\left\{\left[V^{\frac{1}{2}}-V_a^{\frac{1}{2}}\right]^{\frac{1}{2}} V_a^{\frac{1}{2}} - \left[V_a^{\frac{1}{2}}-V_m^{\frac{1}{2}}\right]^{\frac{1}{2}} V_m^{\frac{1}{2}}\, \tfrac{1}{3}\left[V^{\frac{1}{2}}-V_a^{\frac{1}{2}}\right]^{3/2}\right\} - \tfrac{1}{3}\left[V_a^{\frac{1}{2}}-V_m^{\frac{1}{2}}\right]^{3/2}\Bigg\} \qquad \ldots (2)$$

where V_m, the potential minimum, which occurs at $z = L$ is defined by the expression:-

$$\frac{j}{\varepsilon_o}\left(\frac{m}{2e}\right)^{\frac{1}{2}} L^2 = 4\left\{\left[V_a^{\frac{1}{2}} - V_m^{\frac{1}{2}}\right]^{\frac{1}{2}} V_m^{\frac{1}{2}} + \tfrac{1}{3}\left[V_a^{\frac{1}{2}} - V_m^{\frac{1}{2}}\right]^{3/2}\right\}^2 . \qquad \ldots (3)$$

Of particular interest is when $V_m = 0$, which defines the minimum current density (j_o) at which a virtual cathode can exist for given V_a and L:-

$$\frac{jc}{\varepsilon_o}\left(\frac{m}{2e}\right)^{\frac{1}{2}} L^2 = \frac{4}{9} V_a^{3/2} . \qquad \ldots (4)$$

This result can be obtained from Child's Law by considering the virtual cathode situation as two space-charge limited diodes placed back to back.

Dividing equation (3) by equation (4) gives the expression first derived by Bursian and Pavlov (1923):-

$$-\frac{j}{jc} = 4\left(\frac{V_m}{V_a}\right)^{3/2} - 3\left(\frac{V_m}{V_a}\right)^{1/2} - 1 \ . \qquad \ldots (5)$$

$\frac{j}{jc}$ as a function of $\frac{V_m}{V_a}$ is shown in Fig.2. As j is increased, V_m drops along the upper part of the curve; for $j > 2\ j_c$ no solution of equation (5) is possible and the only equilibrium condition is with a virtual cathode ($V_m = 0$) occurring asymmetrically with respect to the grids.

Asymmetric Potential Distribution

In the presence of a virtual cathode there is, in general, only partial transmission of the injected beam; the potential distribution is asymmetric and may be treated as that of two space charge limited diodes back to back, with on one side the sum, and on the other the difference between the injected and reflected current densities (shown schematically in Fig.3).

Applying Child's Law to the regions on each side of the virtual cathode gives:-

$$2j = j_t = \frac{4}{9}\varepsilon_o\left(\frac{2e}{m}\right)^{1/2}\frac{V_a^{3/2}}{Z_c^2} \qquad \ldots (6)$$

and

$$j_t = \frac{4}{9}\varepsilon_o\left(\frac{2e}{m}\right)^{1/2}\frac{V_a^{3/2}}{(2L - Z_c)^2} \qquad \ldots (7)$$

(j_t is the transmitted current density and Z_c the position of the virtual cathode.) Dividing each equation by equation (4) and solving for $\frac{Z_c}{L}$ in terms of $\frac{j}{jc}$ gives:-

$$\frac{Z_c}{L} = 1 - \sqrt{1 - \frac{jc}{2j}\left(1 - \sqrt{1 + \frac{8j}{jc}}\right)} \qquad \ldots (8)$$

From equations (4), (7) and (8) we have:-

$$\frac{jt}{jc} = \left\{\frac{1}{1 + \sqrt{1 + \frac{jc}{2j}\left(1 - \sqrt{1 + \frac{8j}{jc}}\right)}}\right\}^2 \qquad \ldots (9)$$

This relationship, which applies only to the asymmetrical potential distribution becomes imaginary for $j/j_c < 1$. As j/j_c tends to infinity, the virtual cathode approaches the first grid and the system approximates to a space charge limited diode with this grid

as a cathode so that $\frac{j_t}{j_c} \to \frac{1}{4}$. In the case of a symmetric potential distribution (equation 5)) which can exist for $\frac{j}{j_c} \leqslant 2$:-

$$j_t = j .$$

Fig.4 shows $\frac{j_t}{j_c}$ as a function of j/j_c in both the symmetric and asymmetric cases: the sequence ABCDEDFBA, shown in Figs.1b, 2 and 4 illustrates the path taken by the potential minimum and transmitted current density, when the injected current density is taken up to a value greater than $2j_c$ and back to zero. E and B are at the same value of j, but with and without a virtual cathode respectively, as are C and D. As j is increased, V_m drops along the upper part of the curve in Fig.2 and $j = j_t$ in Fig.4. At $j = 2j_c$ a sudden change occurs (C → D) and a virtual cathode is formed at a distance 0.54 L (putting $j = 2j_c$ in equation (8)) from the first grid. Formation is accompanied by a discontinuous fall in j_t from a maximum of $2j_c$ to 0.47 j_c. Further increase in j causes the virtual cathode to move nearer the first grid with a consequent reduction in j_t. If now j is decreased, the virtual cathode moves back toward the midplane of the grids and progressively allows more current to be transmitted as shown by curve (E,D,F) in Fig.4. At $j = j_c$ a rapid relaxation occurs to a higher potential (F → B) without a discontinuous change in j_t. This potential change can be evaluated by solving equation (5) with $j = j_c$ and is equal to $\frac{3}{4} V_a$.

Integration of the electron density between grids, over a potential distribution given by equation (4), yields the total charge per unit area of beam (N_e), current density j_c, containing a virtual cathode:-

$$N_e = \frac{6\, j_c\, L}{e\, U_a} \quad \text{per unit area of beam ,} \qquad \ldots (10)$$

where U_a = velocity of V_a volt electrons. N_e in this case is just three times what it would be if j_c were flowing in the absence of any space charge effects.

Relaxation of a virtual cathode from F → B changes the total charge/unit area by approximately:-

$$\Delta N_e \simeq 3.8 \frac{j_c L}{e\, U_a} \quad \text{per unit area.} \qquad \ldots (11)$$

The change occurs in a few electron transit times.

3. IONIZATION OF RESIDUAL GAS

Of the ion-electron pairs found in the beam, only the ions are retained by the potential well. Their neutralizing effect allows part of the injected electron beam to pass through the space charge without contributing to it, which is equivalent to a reduction in

the electron current density (j) appearing in the space charge equations (2), (5)*.

The virtual cathode relaxation time is the time taken for sufficient ions to accumulate such that the unneutralized current density is reduced to the critical value (j_c).

Transmitted electrons have an ionizing path length 2L whilst those reflected from a virtual cathode have a path length 2 Z_c. Taking this into account, the ionization rate due to the unneutralized part of the beam can be derived from equations (4) (6) (7) and (8) giving:-

$$\frac{N}{t} = \frac{p}{e} \bar{Q} j_c \frac{L}{2}\left[1 + \sqrt{1 + \frac{8j}{j_c}}\right], \qquad \ldots (12)$$

where N is the number of ions/unit area of beam and p the residual gas pressure.

$\bar{Q}$ is an ionizing probability/cm/electron/Torr averaged over a Child's Law potential distribution and is given by:-

$$\bar{Q} = \frac{\int_o^{Va} Q(V)\, V^{-\frac{1}{4}}\, dV}{\int_o^{Va} V^{-\frac{1}{4}}\, dV} . \qquad \ldots (13)$$

where Q(V) is the ionizing probability/cm/electron/Torr for an electron of energy V. Q(V) has been tabulated for various gases (International Critical Tables, Vol.6, p.120). $\bar{Q}$ as a function of V_a is shown for nitrogen in Fig.5.

The neutralized fraction of the beam moves in the space potential without contributing to it. Its path length is 2L so that its ionization rate is:-

$$\frac{\partial N}{\partial t} = 2 \frac{p}{e} \bar{Q} L (j_o - j) , \qquad \ldots (14)$$

where j_o is the total injected current density.

Assuming that each ion neutralizes the space charge of one electron, the neutralized fraction of the beam j' is given approximately by rearranging equation (10) and replacing N_e by N:-

$$j' = \frac{N_e U_a}{6 L} \simeq (j_o - j) . \qquad \ldots (15)$$

This approximation is valid (Volosok and Chirikov 1957) for cases where $N \ll N_e$ and would be exact if the electron and ion spatial distributions coincided.

Differentiation of equation (15) with respect to time yields:-

$$\frac{dj'}{dt} = \frac{e U_a}{6 L} \frac{dN}{dt} . \qquad \ldots (16)$$

*A similar assumption has been made by previous workers.

From (12), (14) and (16):-

$$\frac{dj'}{dt} = \frac{p\,U_a\,\bar{Q}}{3}\left[\frac{j_c}{4}\left(1+\sqrt{1+\frac{8j}{j_c}}\right)+(j_o-j)\right]. \qquad \ldots (17)$$

If $j_o \gg j_c$, reference to Fig.4 shows that initially j_t is almost independent of j so that:-

$$\frac{dj'}{dt} \simeq \frac{dj_t}{dt} \quad \text{(for large } j \text{ or } j_o\text{)} . \qquad \ldots (18)$$

At time $t = 0$, $j = j_o$ which combined with (17) and (18) gives:-

$$\left(\frac{dj_t}{dt}\right)_{t=0} \simeq p\,\frac{U_a\,\bar{Q}}{3}\left[\frac{jc}{4}\left(1+\sqrt{1+\frac{8j_o}{jc}}\right)\right] . \qquad \ldots (19)$$

The initial rate of increase of the transmitted current is thus proportional to pressure: this forms the basis of a method of measuring low pressure proposed by Atkinson (1962b). To achieve the proportionality (19), the currents must be large ($j_o \gg j_c$). However, if $j_o - j_c \ll j_o$ equation (17) reduces approximately to:-

$$\frac{dj'}{dt} \simeq \frac{p\,U_a\,\bar{Q}}{3}\,j_o . \qquad \ldots (20)$$

Integrating equation (20); the time τ at which $j' = (j_o - j_c)$, which is when the virtual cathode disappears, is given by:-

$$\tau = \frac{3\,(j_o - j_c)}{p\,U_a\,\bar{Q}\,j_o} \quad \text{seconds} . \qquad \ldots (21)$$

The relaxation of the virtual cathode is a clearly recognizable event owing to the discontinuous change in potential. τ is inversely proportional to pressure and the determination of τ is the basis of the present proposal for pressure measurement.

4. EFFECT OF FINITE BEAM DIMENSIONS

Consider now a two-dimensional beam derived from a ribbon cathode; this is shown schematically in Fig.6. The grids now form the ends of an equipotential 'box'. We assume that space charge divergence of the beam in the y-direction is prevented by a magnetic field in the z-direction.

It has been shown (7), for a rectangular beam collimated by a magnetic field and containing a virtual cathode, that the potential distribution in the y-direction (in Fig.6) at the virtual cathode, obtained by integration of Poisson's equation (analogous to equations (1) and (4)), is of the form:-

$$V^{\frac{3}{4}} = C_1\,y \quad (C_1 = \text{constant})$$

From this, the electric field at the beam boundary is given by:-

$$\frac{dV}{dy} = \frac{4}{3}\frac{Vb}{d}, \qquad \ldots (22)$$

where V_b = potential at the beam boundary and $2d$ = width of the beam.

Furthermore in the region outside the beam, the potential distribution is of the form:-

$$V = C_2 y \ (C_2 = \text{constant}),$$

and the electric field:-

$$\frac{dV}{dy} = \frac{V_a - V_b}{D - d}, \qquad \ldots (23)$$

(2D is the box width).

At the boundary of the beam, potential and electric field are continuous, so that equating (23) and (24):-

$$\frac{4}{3}\frac{Vb}{d} = \frac{V_a - V_b}{D - d},$$

and for the case of a narrow beam inside a large equipotential box, $(d \ll D)$ this reduces approximately to:-

$$V_b \simeq \frac{3}{4}\frac{d}{D} V_a . \qquad \ldots (24)$$

Under these conditions the potential at the boundary of the beam, in the region of the virtual cathode, is small; in what follows we shall assume that the potential across the beam is uniform. A further assumption is that the potential distribution along the axis of the beam is of the same form as that in a one-dimensional beam:-

$$V^{\frac{3}{4}} = C_3 z, \ (C_3 = \text{constant}),$$

but with the constant C_3 different from that given by Child's Law.

Based on these assumptions, an expression for the potential difference between the first grid and the virtual cathode is derived in terms of geometrical dimensions and j_c^1, the critical current density for virtual cathode formation in a two dimensional beam. Comparison with the one-dimensional case yields a dimensionless equation for the ratio $j_c/j_c{}^1$ in terms only of the beam width to grid separation ratio.

In Fig.6 the contribution to axial electric field at P due to the ribbon of charge Q (extending infinitely in the x direction) is:-

$$dE = 4n\, e \tan^{-1}\left[\frac{d}{(z - z')}\right] dz', \qquad \ldots (25)$$

where n the electron density is a function of z':-

$$n = \frac{jc' (L)^{2/3}}{e\, Va\, z'^{2/3}},$$

and the contribution to potential change in moving from the first grid (L) to the virtual cathode due to this charge filament is:-

$$dV = \int_{L}^{o} dE\, dz \quad . \qquad \ldots (26)$$

Substituting for the electric field and summing over the space between the grids:-

$$V_a = \int_{-L}^{+L} \int_{L}^{o} \frac{4\, jc^1\, L^{2/3}}{V_a\, z'^{2/3}} \tan^{-1}\left[\frac{d}{(z - z')}\right] dz'\, dz \quad . \qquad \ldots (27)$$

Dividing (27) by equation (4) and integrating once gives:-

$$\frac{jc}{jc^1} = \tfrac{1}{3}\pi \int_{-1}^{+1} \left\{ \frac{(1-\alpha)}{\alpha^{\frac{2}{3}}} \tan^{-1}\left(\frac{\beta}{1-\alpha}\right) - \alpha^{\frac{1}{3}} \tan^{-1}\left(\frac{\beta}{\alpha}\right) + \frac{\beta}{2\alpha}\frac{2}{3} \ln\left(\frac{\beta^2 + (1-\alpha)^2}{\beta^2 + \alpha^2}\right) d\alpha, \right. \qquad \ldots (28)$$

where

$$\alpha = \frac{z}{L} ,$$

and

$$\beta = \frac{d}{L} .$$

$\frac{jc^1}{jc}$ is a function of $\frac{d}{L}$ only and is shown in Fig.7. As $\frac{d}{L} \to 0$, $\frac{jc^1}{jc} \to \infty$ and as $\frac{d}{L} \to \infty$, $\frac{jc^1}{jc} \to 1$.

Combining equation (4) with the computed curve for $\frac{jc^1}{jc}$ we get:-

$$jc^1 = \frac{4}{9}\, \varepsilon o \left(\frac{2e}{m}\right)^{\frac{1}{2}} \frac{V_a^{3/2}}{L^2} \left(\frac{jc^1}{jc}\right) , \qquad \ldots (29)$$

from which we derive the critical current/cm of filament:-

$$I_c{}^1 = \frac{4}{9}\, \varepsilon o \left(\frac{2e}{m}\right)^{\frac{1}{2}} V_a{}^{3/2} \left\{ \frac{d}{L^2} \left(\frac{jc^1}{jc}\right) \right\} \text{ amps/cm} . \qquad \ldots (30)$$

In Fig.8 this function is plotted against 2L for two values of 2d.

5. INSTABILITY

In the final stages of space charge neutralization, the electron beam passing through the accumulated ions might be expected to excite "two-stream" type electrostatic instabilities. The preferential growing space period of the simplest instability is given by (for example, Buneman 1959),

$$\lambda = \frac{2\pi u}{\omega_{pe}} , \qquad \ldots (31)$$

where u is the electron beam velocity. The usual expression for ω_{pe} the electron plasma frequency, is based on a plasma of infinite extent. If we assume that under finite conditions, the electric field tending to restore an electron displaced in the z-direction

from its equilibrium position is reduced by a factor F, then the expression for ω_{pe} becomes:-

$$\omega_{pe} = \left(\frac{n_e e^2}{\varepsilon_o m F} \right)^{\frac{1}{2}} . \qquad \ldots (32)$$

This reduction of the electric field in the beam by a factor F is also responsible for the increase in j_c when changing from the case of a one-dimensional beam to that of a finite (or two-dimensional) beam, (c.f. equation (27)) so that:-

$$F = \frac{j_c \text{ in a finite beam (or } j_c{}^1)}{j_c \text{ in a one dimensional beam}} .$$

If it is assumed that the instability will appear when its spatial period λ is comparable with the electron beam 'length' (i.e. $\lambda \sim 2L$), and also that the mean electron velocity and density in the virtual cathode are given respectively by:-

$$\left.\begin{aligned} u &= \frac{u_a}{3} \\ n_e &= \frac{j}{e\,u} \end{aligned}\right\} \text{ (analogous to equation (10))} \qquad \ldots (33)$$

then an expression for the current density at which the instability will appear (j*) is obtained from equations (32), (33) and (34):-

$$j^* \sim \frac{\pi^2 \varepsilon_o U_a{}^3 m F}{27 e L^2} \text{ amps/unit area} . \qquad \ldots (34)$$

Dividing this expression by equation (29), and considering F equivalent to $\frac{j_c{}^1}{j_c}$, yields the interesting condition:-

$$j^*/j_c{}^1 \sim \frac{\pi^2}{6} \simeq 1.7 . \qquad \ldots (35)$$

This approximate result should be equally valid for one, two or three-dimensional beams.

6. DESIGN OF A VACUUM GAUGE

We now consider the application of the foregoing ideas to the design of a practical vacuum gauge.

It is desirable in a high vacuum system that thermal dissipation should be kept to a minimum to reduce outgassing. From Fig.7 we see that I_c decreases with increasing L, and is almost independent of d in the range 0.2 to 2mm. For this reason L should be made as large as is consistent with stable operation and the space available. Temperature limitation of emission from the filament is necessary in order that the beam current may be varied independently of accelerating voltage and also to minimise the effect of residual gas ions in the electron gun.

The choice of electron accelerating potential is a compromise between, on the one hand

increased ionizing efficiency at high voltages ($\bar{Q}$ as a function of V_a is shown in Fig.5) and on the other hand the lower thermal dissipation, both from filament and electron beam ($\alpha V_a^{5/2}$), obtained at lower voltages.

Since from equation (21) the gauge constant:-

$$\tau p \propto \frac{j_o - j_c}{j_c} ,$$

and from equation (4) $j_c \propto V_a^{3/2}$, stabilization of both the emission current and voltage are necessary.

Divergence of the beam due to the radial electric field at the virtual cathode can be minimised by a suitable magnetic field. Assuming that this will limit the beam spread to the order of an electron Larmor radius, then for this to be unimportant, the required magnetic field strength B is given by:-

$$B \gg \frac{u\, m}{d\, e} \qquad \ldots (36)$$

where u is the average electron velocity.

This field will similarly prevent the residual gas ions with their near thermal velocities from having appreciable Larmor radii.

Fig.9 shows a schematic diagram of a practical gauge with its associated equipment. Electrons from a directly heated tantalum cathode are accelerated by a 60 volt square wave, at 10 c/s, into a conducting box anode, 2.5 cm long, with mesh sides. In the present case the cross-section of the beam is approximately 2.5 mm × 1.2 cm and of the conducting box 3 cm × 3 cm. Changes in the total charge inside the box are detected by an electrostatic probe which consists of a conducting mesh ring just inside the mesh wall of the box and encircling the beam. It is connected electrically to the box anode through the 1 MΩ input resistance of an oscilloscope with a 200 pF connecting lead capacitance in parallel. An axial magnetic field of up to 8 kG is provided by an external solenoid. The field required to satisfy (37) was given by:-

$$B \gg 200 \text{ gauss.}$$

The complete circuit for the required voltage and emission stabilization is shown in Fig.10.

7. EXPERIMENTAL PROCEDURE AND RESULTS

All pressure measurements were made with a magnetically screened Bayard-Alpert type ionization gauge (Mullard IOG 4) in an oil-pumped stainless steel vacuum system (Fig.11) which could be baked to 450°C, achieving a base pressure of 5×10^{-10} Torr. Nitrogen or other gases could be admitted through a needle valve from a reservoir, with liquid air trap, maintained at between 1 and 10^{-3} Torr, which in turn was fed through a second needle valve from a cylinder of nitrogen. This differential leak system provided fine control over the main system pressure in the range 10^{-4} to 5×10^{-10} Torr.

Fig.12 shows a typical oscillogram of the pulses appearing on the electrostatic probe compared with the H.T. waveform. A negative pulse of magnitude 0.3 volts and a microsecond rise-time appears at the establishment of the beam. After time τ a positive pulse appears with rise-time less than a microsecond corresponding to destruction of the virtual cathode.

From the geometry one would anticipate that about one quarter of the change in total charge within the 'box', estimated from equation (11), would be detected on the 200 pF electrostatic probe: the expected magnitude of the pulse would then be ~ 65 mV: in practice, however, it is in the region of 30 mV. As expected the magnitude is independent of pressure.

As the emission current I_o is reduced, τ tends to zero, independently of pressure. If one assumes that a relationship between I_o and minimum potential, similar to that illustrated in Fig.2, exists, then it is at first sight surprising that vanishingly small τ can be observed. One might expect the virtual cathode formation current to bear a definite relationship (a factor between 1 and 2) to its destruction current I_c, which in turn implies through equation (21), that there should be a finite minimum value of τ dependent on pressure. We have seen, however, that I_c is dependent on $V_a^{3/2}$, so that at some stage during the H.T. turn-on, conditions for virtual cathode formation will be satisfied. This is further confined by the existence, at emission currents just below the critical current, of a small relaxation step occurring within microseconds of the turn-on, which is independent of pressure and is probably due to a virtual cathode formed during the H.T. turn-on at an intermediate accelerating potential, relaxing when the steady value is reached. The current at which τ becomes zero (I_c) has been measured for accelerating potentials in the range 45 to 65 volts, and over this range agrees with the empirical equation (related to equation (4)) shown in Table I. For comparison, the relationship between I_c and V_a

calculated for the same filament dimensions using the two dimensional theory (Fig.8) and the one-dimensional theory (equation (4)) are shown:-

TABLE I

Relationship between Critical Current I_c and Accelerating Potential V_a for a Beam of Cross Section 2.5 mm × 1.2 cm and 'box' Length 2.5 cm

Experimental	$I_c = 7.5 \times 10^{-6} V_a^{3/2}$ amps (within 5%)
Two dimensional theory (Fig.8)	$I_c = 5.5 \times 10^{-6} V_a^{3/2}$ amps
One dimensional theory (Eq. (4))	$I_c = 0.45 \times 10^{-6} V_a^{3/2}$ amps

Increasing I_o gives rise to an abrupt change in the probe signal, characterised by repeated bursts of high frequency (> 1 Mc/s) oscillation after the initial relaxation. This transition is illustrated by Fig.13, an oscillogram comparing the probe signals at an I_o of $1.7\ I_c$ (upper trace) and $1.8\ I_c$ (lower trace), both taken at a pressure of 10^{-6} Torr. The value of I_o at which the change occurs is dependent on pressure and is typically $\sim 1.5\ I_c$ at 10^{-8} Torr rising to $\sim 2.0\ I_c$ at 10^{-5} Torr. These values are in reasonable agreement with the predictions of equation (35) for the onset of a two-stream electrostatic instability. All present measurements were made at currents below this region.

Measurements of τ against emission current made at two fixed pressures, shown in Fig.14, are in good agreement with the behaviour expected from equation (12) and show clearly that I_c is independent of pressure. Measurement of I_c provides an easy way of checking that the dimensions of a particular gauge have been maintained and hence the calibration holds.

8. RELAXATION TIME AND MAGNETIC FIELD

Variation of the axial magnetic field strength from 0 to 8 kG changed τ as shown in Fig.15. τ was independent of field strength above 1.8 kG, but reliable operation could be achieved down to 0.3 kG. Below 0.3 kG, divergence of the beam was such that a virtual cathode could not be formed without increasing emission current, whilst at lower field still, part of the beam apparently intercepted the electrostatic probe.

Alignment of the gauge with the magnetic field is not critical with the present geometry, and an earlier gauge was operated satisfactorily with a permanent magnet supply of 1 kG field of doubtful uniformity.

9. RELAXATION TIME AND PRESSURE

With a fixed emission current of 4.3 mA and accelerating potential of 60 volts, τ has been measured between 6 μsec and 66 msec (Fig.16) and found to be inversely proportional to pressure in the range 5×10^{-5} to 4×10^{-9} Torr nitrogen pressure, within 10%. The measured gauge constant (τp) was 3×10^{-10} Torr seconds for nitrogen, whilst that given by putting the measured critical current of 3.5 mA and $\bar{Q}$ (Fig.5) for nitrogen into equation (12) was 4×10^{-10} Torr seconds.

The gauge constant (τp) is reproducible to better than 5% when both the voltage and emission current are stabilized to ~ 1%.

The high pressure limit to operation is the beam 'turn on' time. This consists of two factors; the time for the first few electron transists in the box, which in the present case is ~ 10^{-7} sec, and the risetime of the H.T. voltage pulse which is ~ 10^{-6} sec. At pressures above ~ 5×10^{-5} Torr, τ became comparable with the H.T. risetime and consequently measurements became progressively more inaccurate.

A low pressure limit has not been determined, but if due solely to dissociative recombination should be better than 10^{-11} Torr assuming a recombination cross section $\sigma < 10^{-19}$ cm^2.

Measurements at pressures in the range 10^{-8} to 10^{-9} Torr were repeatable but a definite deviation from linearity was observed. It was found that if the time between operations of the gauge at constant pressure was increased to the order of 100 msec, τ approached a limiting value as shown in Fig.17 and linearity was largely restored to the curve in Fig.16.

Each cycle of the gauge's operation accumulated ~ 10^8 ions, which, unless given time to disperse, give rise to an apparent local increase in pressure. This is further supported by the observation that increasing the 'on' time of the beam (and therefore the amount of ionization) also has an adverse effect on linearity of τ with pressure < 10^{-8} Torr. The time for neutralized ions to diffuse out of the box anode, due to their thermal velocities is at the most the order of 200 μsec. As the ions can only escape from the box via the end electrodes where they are neutralized, it appears that temporary adsorption (for ~ 100 msec) takes place on these very clean electrodes after the electron beam is turned off, only to be released again during the next cycle if this occurs before ~ 100 msec. This behaviour suggests that at very low pressures, 'one shot' operation would be preferable.

At pressures near the base pressure of the system (5×10^{-10} Torr) measurements of τ were unreproducible and varied over a period of time in a way that suggested outgassing of

the electrode structure. Further minor deviations may be attributable to changes in composition of the residual gases near the base pressure of the vacuum system.

10. GAS CORRECTION FACTORS

A number of pressure comparisons were made, in the range 10^{-6} to 10^{-8} Torr in nitrogen, hydrogen and argon. After applying gas correction factors to the IOG.4 ionization gauge used as a standard, the measured gas correction factors normalised to nitrogen for the virtual cathode gauge are shown in Table II, compared with the predictions of equation (13):-

TABLE II

Gas Correction Factors for the Virtual Cathode Gauge with 60 Volts HT

	Hydrogen	Nitrogen	Argon
Calculated	2.35	1	0.83
Measured	2.4 ± 0.1	1	0.9 ± 0.1
IOG.4	2.5	1	0.75

11. RELAXATION OSCILLATIONS

Regular, spontaneous relaxation oscillations were observed at the electrostatic probe if the electron beam remained on much longer than the initial relaxation time. Fig.18 shows an oscillogram of oscillations, obtained with the H.T. on continuously, whose frequency increased with pressure although not apparently linearly over the same pressure range as the preceding measurements. These oscillations, which occur over a limited range of emission current, are consistent with a potential minimum - emission current density curve similar to that in Fig.2 in which ions are spilled out of the virtual cathode at the relaxation (E → B) thus allowing it to reform. This effect has not been fully investigated.

12. A PRACTICAL APPLICATION

Although circuitry could be devised to convert τ into a direct pressure reading, it has been found convenient when studying pressure transients to display the pulses defining τ on an oscilloscope. The sharp voltage pulse from the electrostatic probe, which signifies the destruction of the virtual cathode is differentiated and amplified, and made to 'bright-up' the trace on a C.R.O. with two timebases. The y-timebase is triggered by the H.T. turn-on and scans at a rate determined by the pressure range whilst the other scans

slowly in the x-direction. The brightened spot traces a line which enables τ to be continuously measured. Fig.19 is an oscillogram showing variation in τ over a 10 second period during the operation of an ion-injection magnetic mirror trap. Note the fall in pressure when the ion injection is turned off.

13. CONCLUSIONS

The principle feature of the present method of measuring very low pressures is that it requires only a measurement of a time interval between two pulses and avoide the necessity for measuring very small currents, as in conventional ionization gauges. With an emission current of 4.3 mA, virtual cathode relaxation time has been found to be inversely proportional to residual gas pressure in the range 5×10^{-5} to 4×10^{-9} Torr within 10%.

Although a magnetic field is necessary for operation, τ is independent of magnetic field strength above 1.8 kG which is of value when pressure measurements are required in the presence of strong magnetic fields. Because the magnitude of the pulses defining the relaxation time is independent of pressure, the gauge is insensitive to leakage currents and to electrical pick-up which can usually be differentiated from the fast pulses. A prototype gauge has run for more than 200 hours over a period of months and has given consistent pressure measurements throughout this time.

14. ACKNOWLEDGEMENTS

The author wishes to thank Dr. A.E. Robson for his encouragement and advice, Dr. H.H. Atkinson for the suggestion on which the work was based and M.J. Terry for his competent assistance.

15. REFERENCES

ATKINSON, H.H., 1962 a, Proc. 4th Int. Congress on Microwave Tubes, September, 1962. Eindhaven, Centrex Pub. Co., 1963. p.559.

ATKINSON, H.H., 1962 b, Cograte Brit. Patent Application nos.33664/62 and 12083/63.

ATKINSON, H.H., 1963, Trans. 10th National Vacuum Symposium, October, 1963. New York, Macmillan, 1964. p.213.

BUNEMAN, O., 1959, Phys. Rev., 115, 503.

BURSIAN, V. and PAVLOV, V., 1923. Zh. Russ. Fiz. Khim. Obshchestoi, 55, 71.

INTERNATIONAL CRITICAL TABLES. New York, McGraw-Hill, 1929, 6, 120.

HAEFF, A.V., 1939, Proc. Inst. Rad. Engrs, 27, 586.

VOLOSOK, V.I. and CHIRIKOV, B.V., 1957, Zh. Tech. Fiz., 27, 2624. (Trans. in Sov. Phys.-Tech. Phys., 1958, 2, 2437)

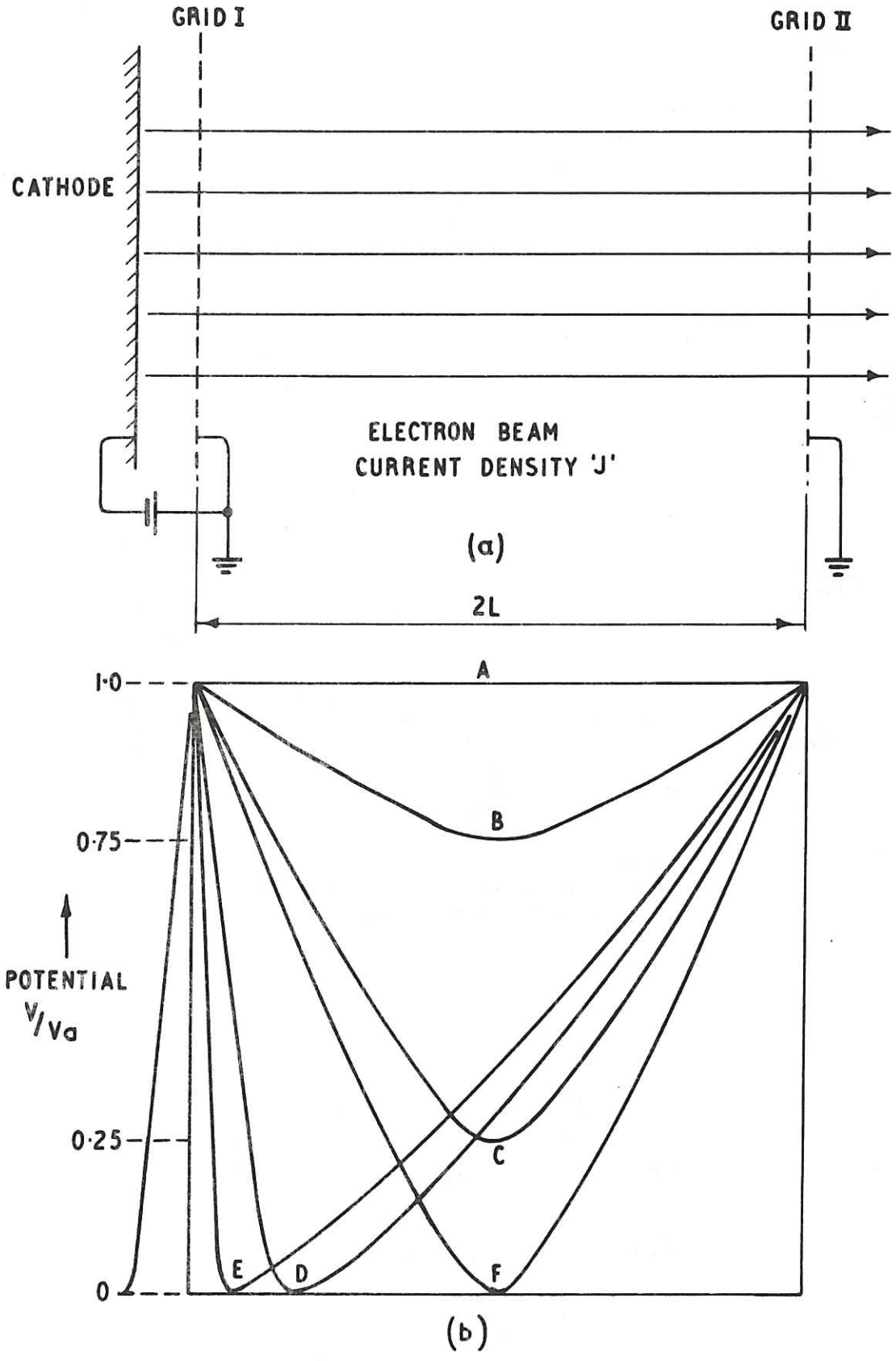

Fig. 1 (CLM-P80)
(a) Schematic diagram of the one-dimensional beam with
(b) potential distributions at different current densities

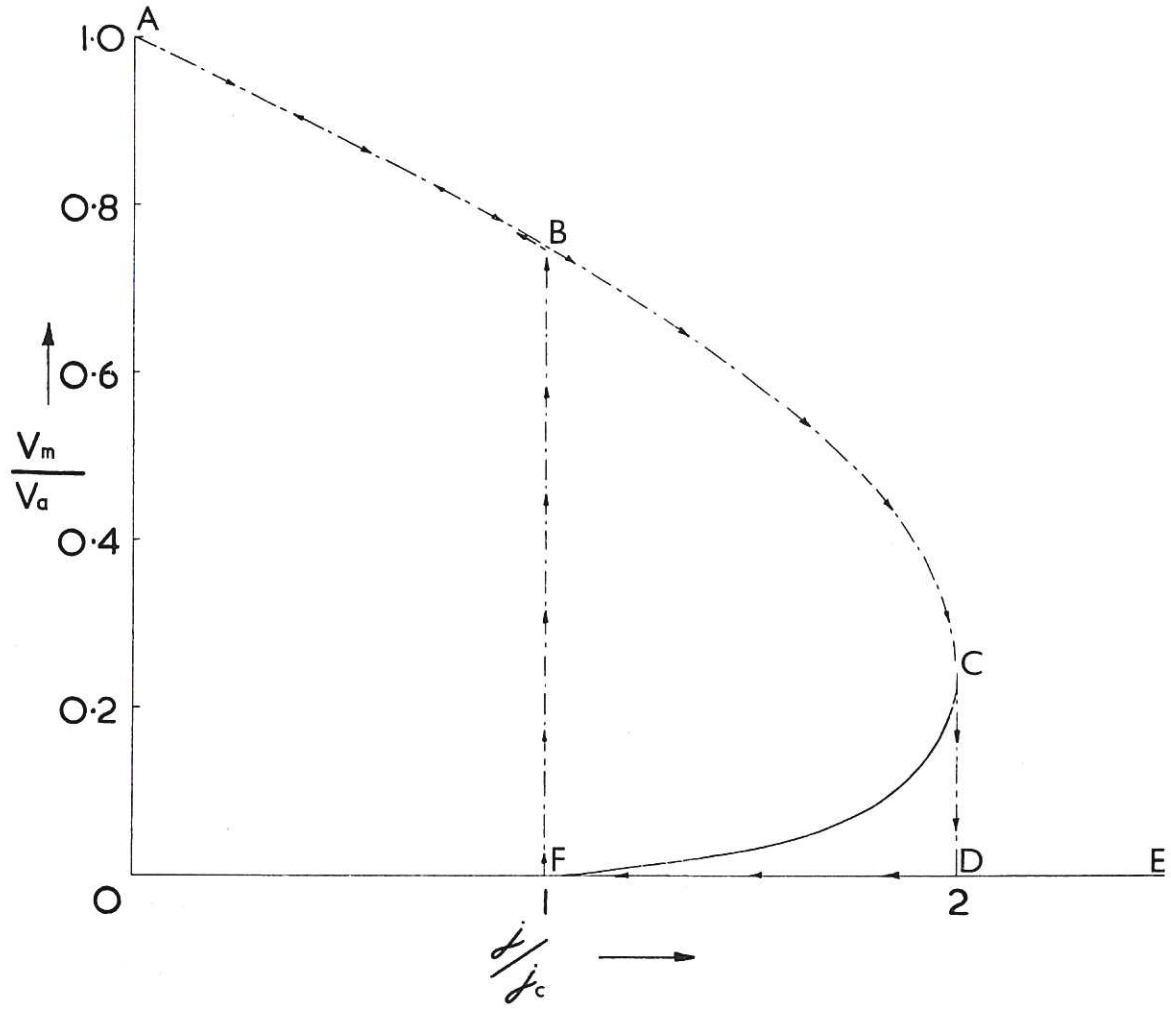

Fig. 2 (CLM-P 80)
Relationship between minimum potential and injected current density in a one-dimensional beam

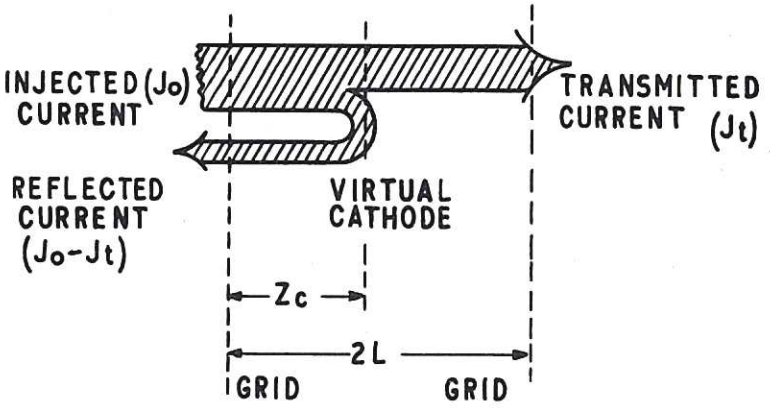

Fig. 3 (CLM:-P 80)
Schematic diagram of current flow in the presence of a virtual cathode

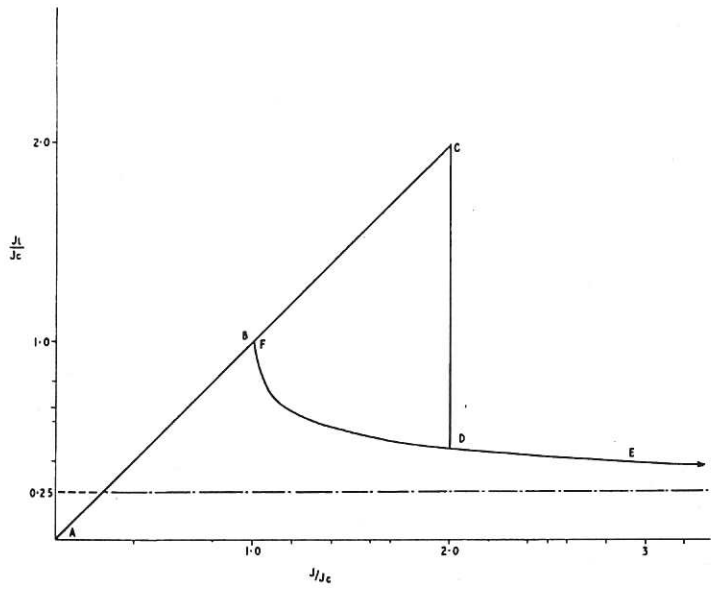

Fig. 4 (CLM-P80)
Relationship between injected and transmitted current densities in a one-dimensional beam

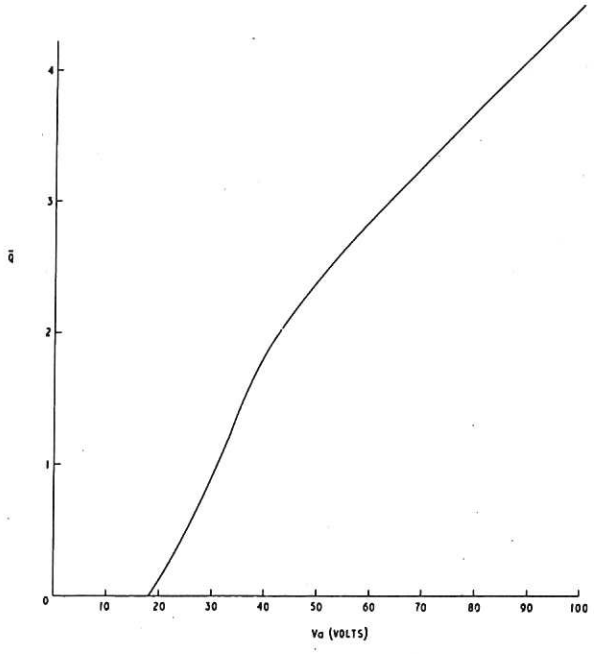

Fig. 5 (CLM-P80)
Ionizing probability/cm/electron/Torr in nitrogen averaged over a virtual cathode potential distribution ($\bar{Q}$) as a function of the electron accelerating potential (V_a)

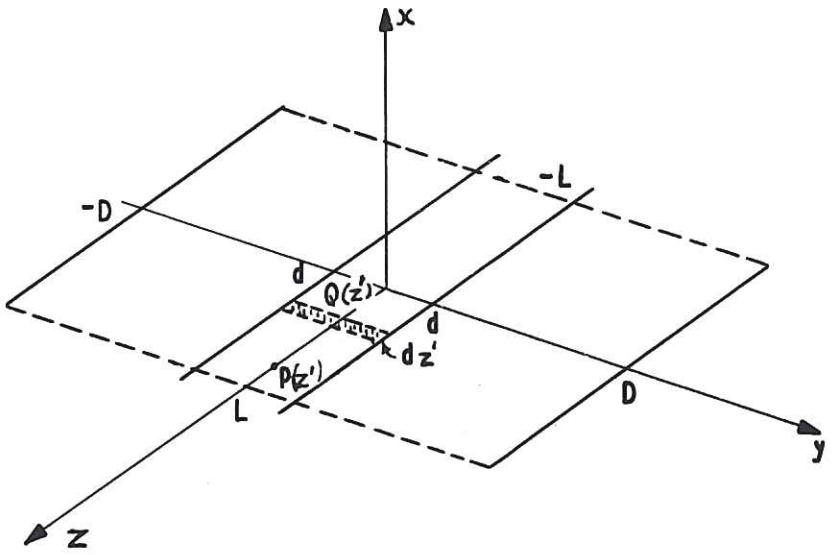

Fig. 6 (CLM-P80)

Cross-section through a two-dimensional beam which extends infinitely in the x-direction, and is defined in the y-direction by the planes $y = \pm d$. The direction of current flow is parallel to the z-axis and is bounded by equipotential grids in the planes $z = \pm L$. These grids are connected to conducting walls in the planes $y = \pm D$

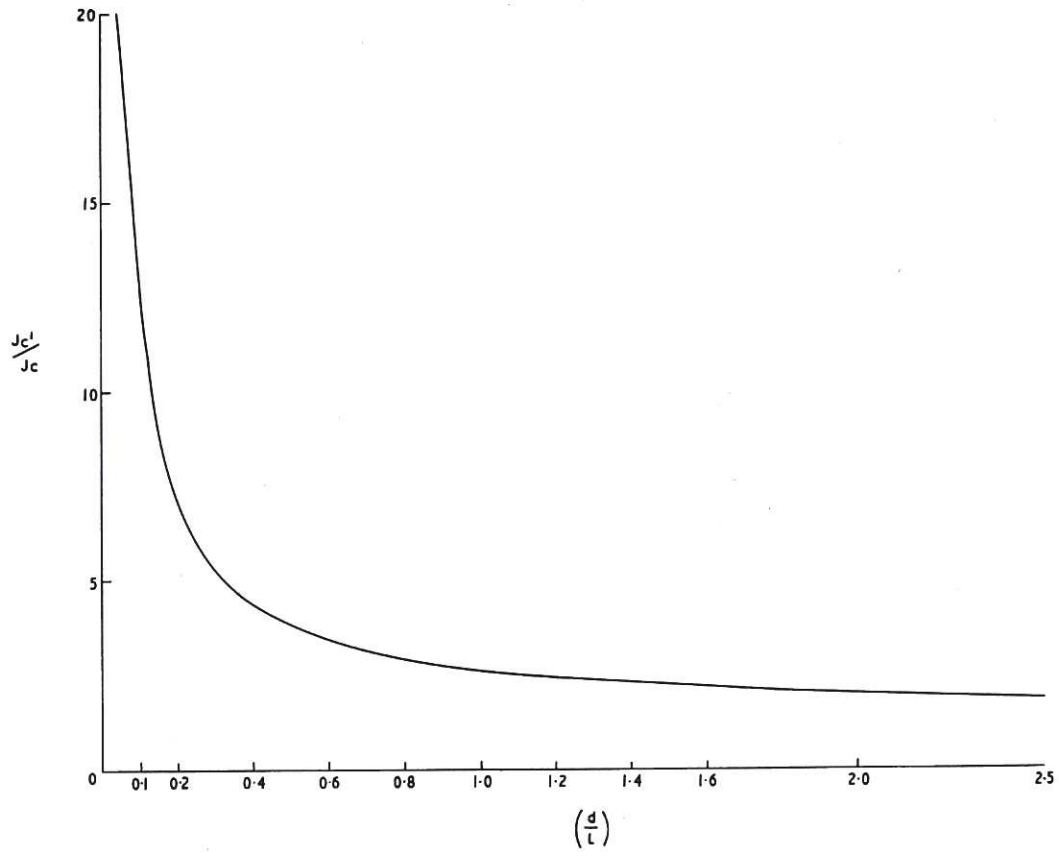

Fig. 7 (CLM-P80)

Computed relationship between the increase in virtual cathode destruction current in a two-dimensional beam (compared with a one-dimensional beam) and the ratio of beam width to grid spacing (d/L)

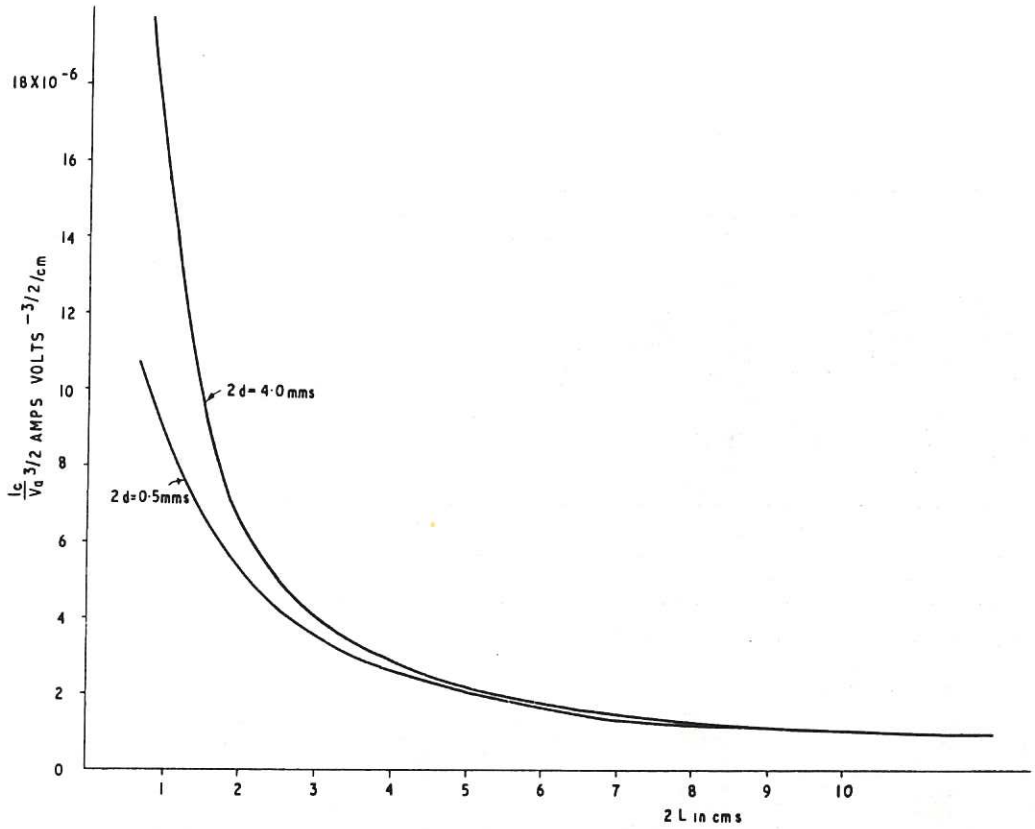

Fig. 8 (CLM-P80)

Virtual cathode destruction current per cm. of two-dimensional beam as a function of grid spacing (2L) for two values of beam width (2d)

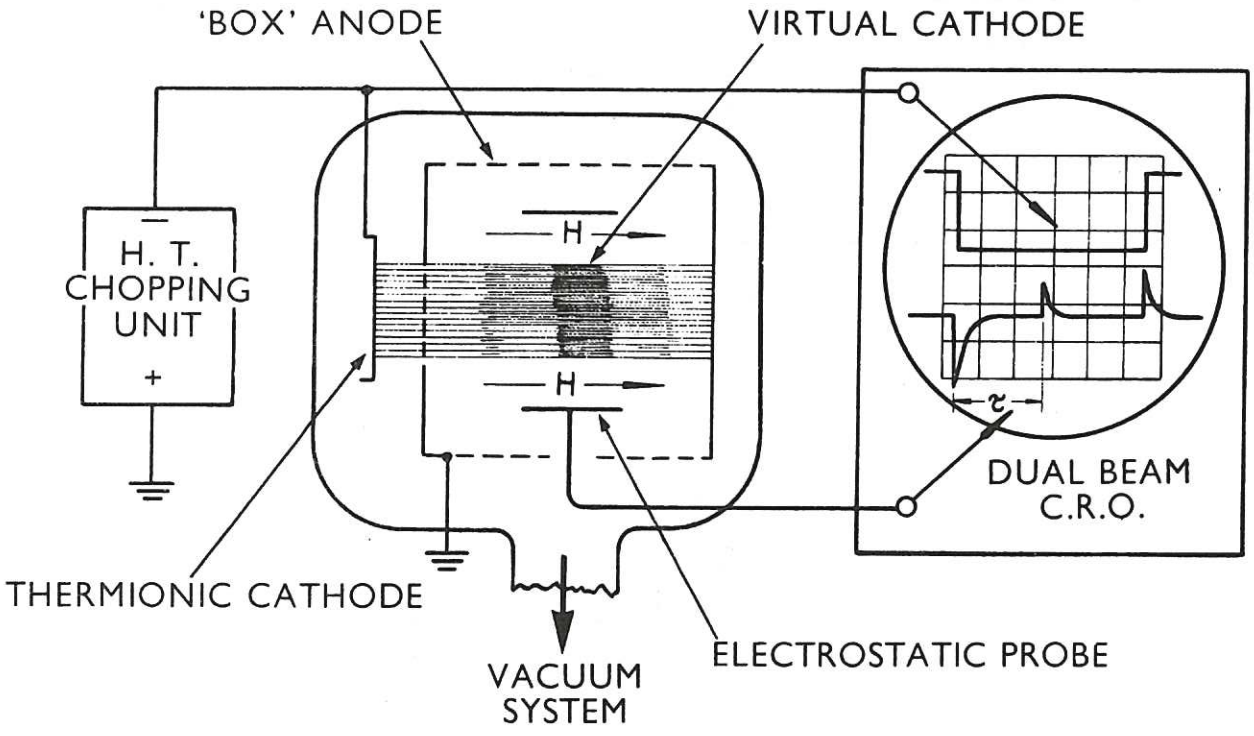

Fig. 9 (CLM-P80)

Schematic diagram of a practical gauge with its associated equipment

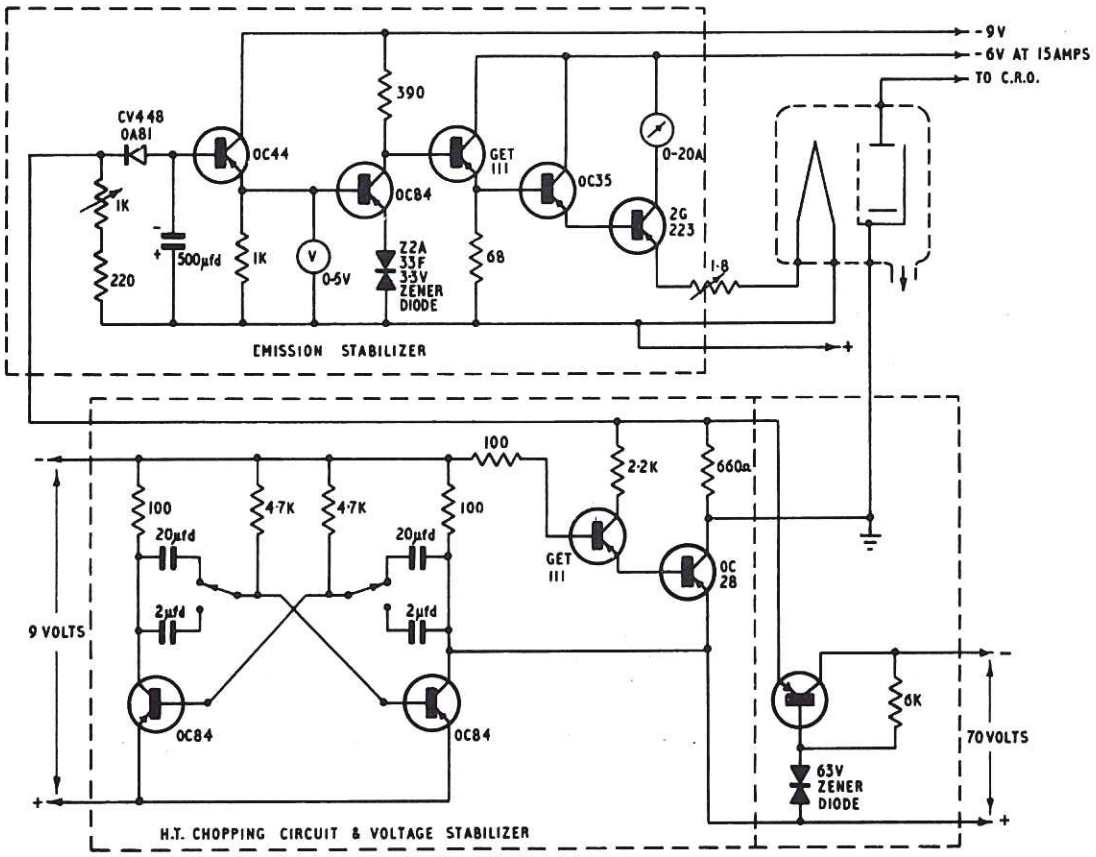

Fig. 10 (CLM-P80)
Diagram of H.T. chopping circuitry, and voltage and emission current stabilizer

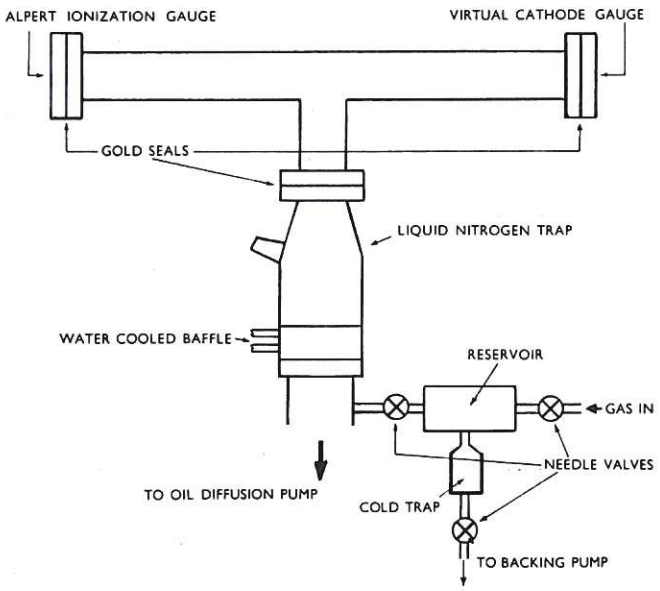

Fig. 11 (CLM-P80)
Layout of the vacuum system

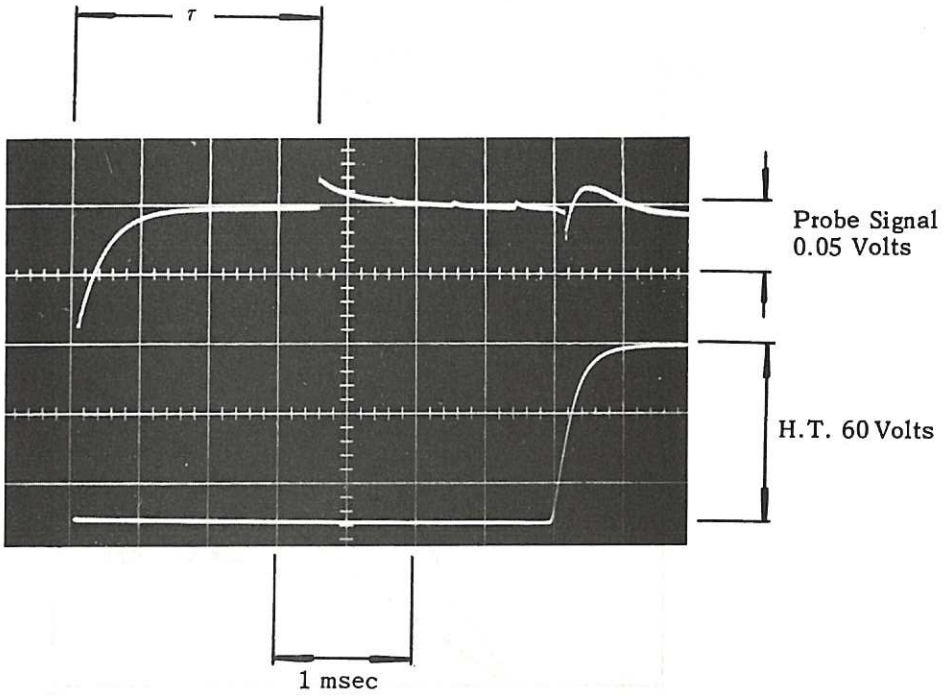

Fig. 12 (CLM-P80)
Oscillogram of a typical electrostatic probe signal, showing the virtual cathode relaxation (upper trace), compared with the H.T. waveform

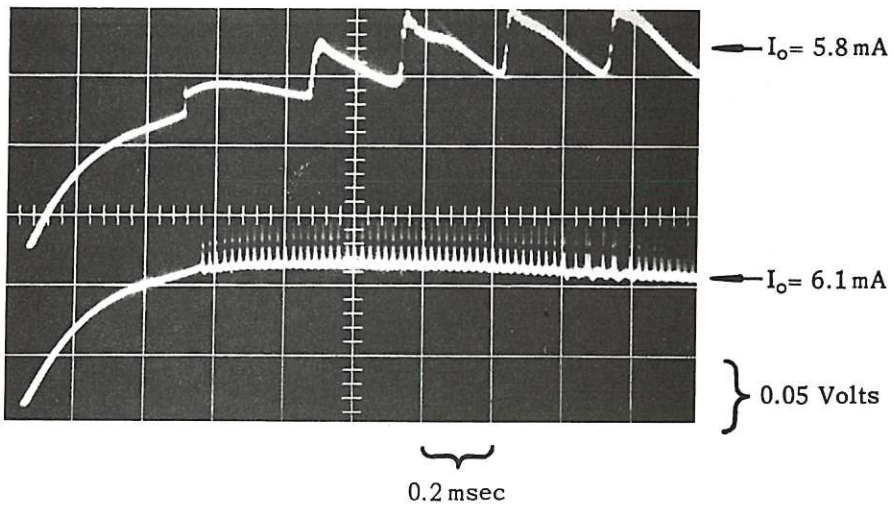

Fig. 13 (CLM-P80)
Oscillogram comparing probe signals at emission currents (I_o) close to the instability threshold

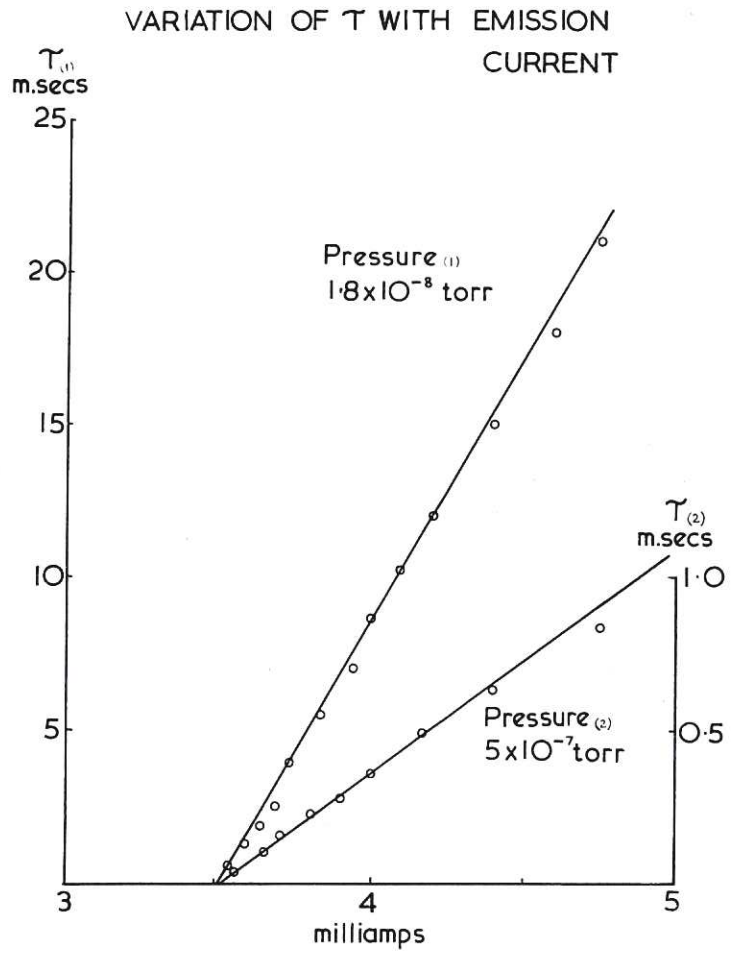

Fig. 14 (CLM-P80)
Measurements of virtual cathode relaxation time τ against emission current I_0 at two fixed pressures

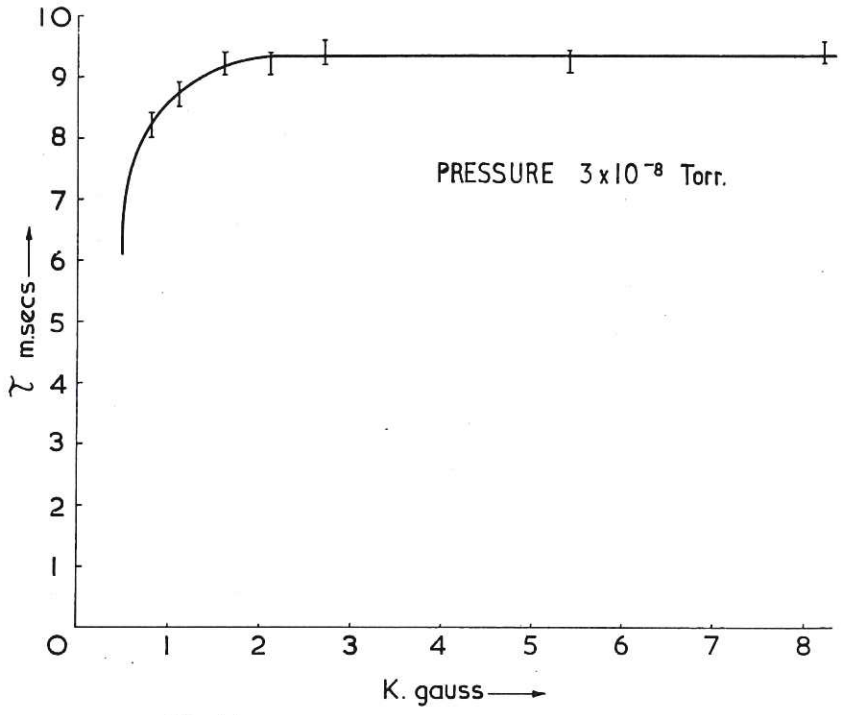

Fig. 15 (CLM-P80)
Variation of virtual cathode relaxation time τ with magnetic field strength

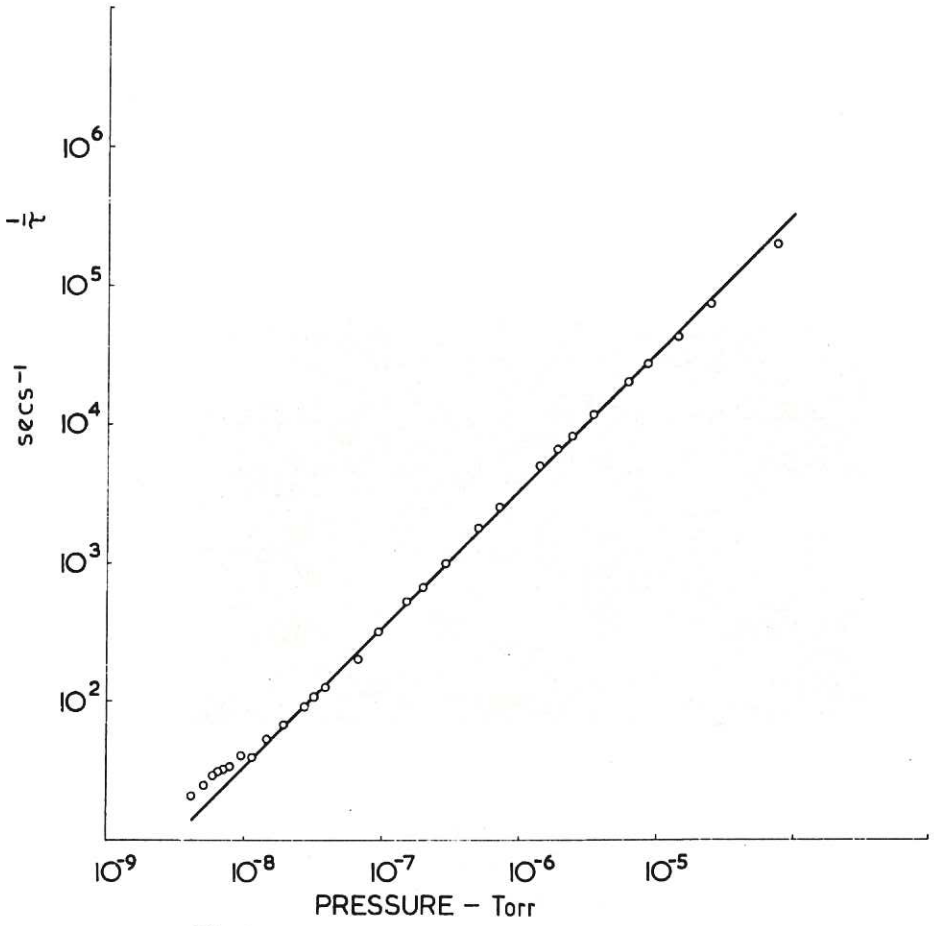

Fig. 16 (CLM-P80)
Variation of inverse virtual cathode relaxation with gas pressure (measured by an Alpert ionization gauge)

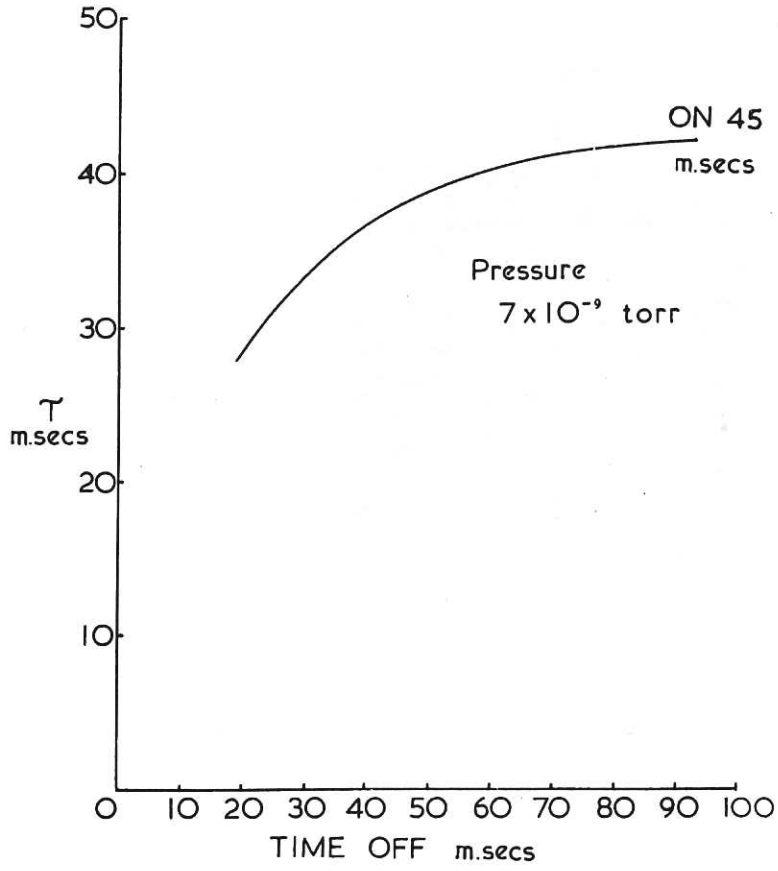

Fig. 17 (CLM-P80)
Showing the variation in τ as the time between 45msec H.T. pulses is increased

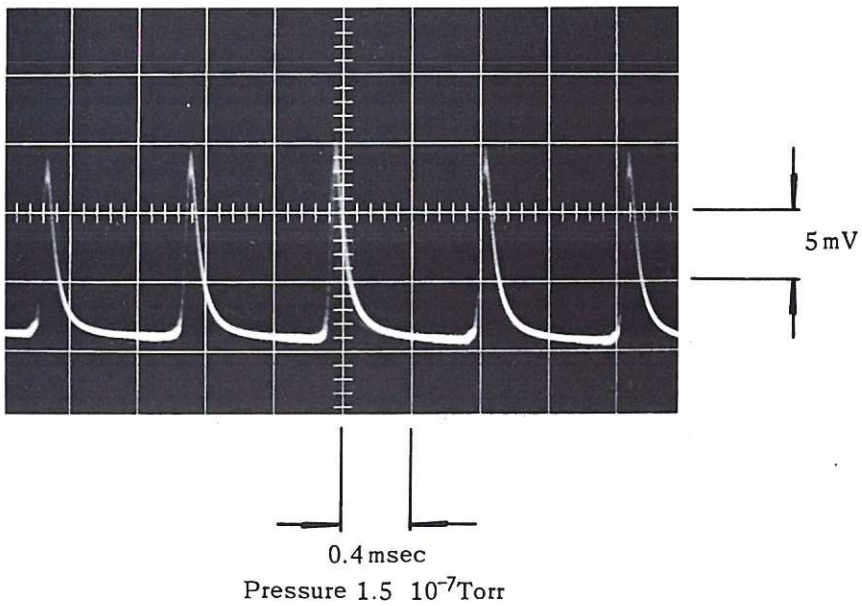

Fig. 18 (CLM-P80)
Oscillogram of the probe signal obtained under certain conditions with the H.T. on continuously

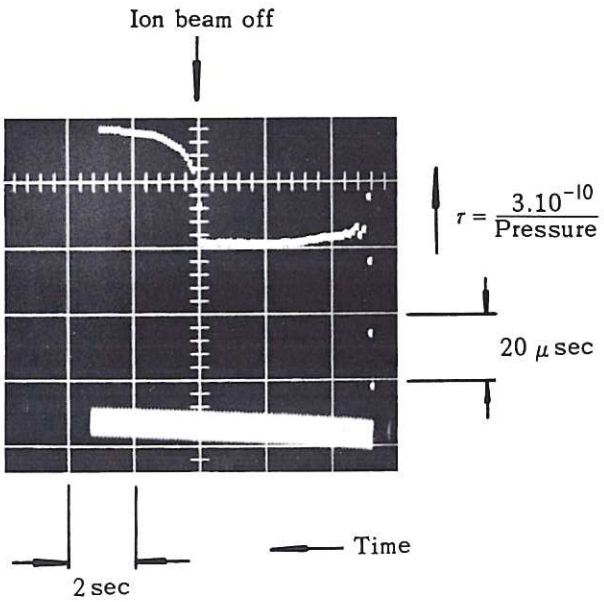

Fig. 19 (CLM-P80)
Illustrating a method of using the virtual cathode gauge for time resolved pressure measurements in a magnetic mirror machine